Dear Editors and Reviewers,

We apologize for not fully addressing your revision requests in our previous responses. We sincerely appreciate your meticulous review of our manuscript egusphere-2024-930. In response to your feedback, we have made significant and careful revisions, particularly concerning the validation of the methods used in this study. The revised portions are marked in the revised manuscript. Please find our responses to the reviewers' comments as follows:

Responses to the reviewer #1

[This work investigates the stratosphere-to-troposphere transport (STT) processes based on pure trajectory simulations; however, reasonable validations of trajectory are totally absent. The representation of tropopause is a fundamental factor controlling where and how stratospheric air enters the troposphere, but it is poorly resolved in the manuscript that simply uses two fixed PV thresholds over very broad regions. Therefore, detailed validations of simulations against observations are essentially important for the reliability of results. Though the authors provide some comparisons with TOST ozone data, the coarse temporal and spatial resolution of TOST is not able to track the fine-scale features of STT.]

Response 1: We appreciate the reviewer's constructive comments and agree that detailed validation of simulations against observations are indeed essential for ensuring the reliability of the results. Given the inherent challenges in observing stratospheric ozone in the troposphere, assessing stratospheric intrusions and their vertical structure is particularly difficult. To address this concern, we have undertaken extensive validations and revisions to improve our paper as follows:

1. **Comparing the spatial structure of simulated SI ozone with Aura OMI data:** We compared the spatial distribution of simulated SI ozone with tropospheric ozone observations from the OMI remote sensing data (in Section 2.4). The vertical variations of OMI and SI ozone exhibit similar spatial patterns over CEC in the troposphere, while the simulated SI ozone concentrations are notably lower than those observed by OMI. This comparison underscores the reasonable relationships between stratospheric impact and total ozone (SI + tropospheric production) in the troposphere, thereby validating the reliability of our simulation methodology.
2. **Examining correlations with stratospheric ozone tracers:** We evaluated the correlation between simulated SI ozone and two stratospheric ozone tracer reanalysis datasets (EAC4 and CAM). This comparison, detailed in Section 2.4, shows a strong correlation, with coefficients in most sub-regions exceeding 0.7 and passing the confidence threshold of 99.9%.

3. **Comparison with ground-based observations:** We compared the SI events identified in our simulations with those identified from ground-based records. This analysis, presented in Section 3.3, demonstrates that our simulations achieve a high hit rate for SI events across nearly all sub-regions, indicating that our methodology effectively identifies SI events at the ground level.
4. We have removed the comparison with TOST data, as the TOST dataset was too coarse to be appropriate.

- The comparisons with OMI satellite data and stratospheric ozone tracer reanalysis datasets are detailed in Section 2.4 (Lines 210-247):

2.4 Validation of the Lagrangian simulations

Validating the stratospheric trajectories and associated vertical profiles of ozone is crucial for understanding the key features of stratospheric intrusion (SI) events. Given the challenges in observing stratospheric ozone in the troposphere, assessing stratospheric intrusions and their vertical structure is inherently difficult. We validated the reliability of our FLEXPART simulations for stratospheric trajectories in the troposphere by comparing simulated daily SI ozone with stratospheric ozone tracers from two reanalysis datasets of atmospheric compositions, as well as the satellite remote sensing of tropospheric ozone.

2.4.1 Comparisons with stratospheric ozone tracers

Although continental-scale tracer experiments offer unique opportunities to test Lagrangian simulations, few such experiments have been conducted (Stohl et al., 1998). Here, we employed two reanalysis datasets (EAC4 and CAM) containing O_3S as alternatives to analyze correlations with SI ozone from May to August 2019 simulated across six sub-regions, as depicted in the boxes of Figure 3e. EAC4 and CAM have horizontal resolutions of $0.75°\times0.75°$ and $0.9°\times1.25°$, respectively, and are capable of resolving daily SI processes. We performed two cross-validations (FLEXPART vs EAC4 and FLEXPART vs CAM) of stratospheric ozone intrusion and transport in the troposphere. Figure 1 shows strong correlations between SI ozone and the two O_3S datasets, with correlation coefficients in most sub-regions exceeding 0.7 and meeting the confidence threshold of 99.9%. Although the magnitude of O_3S in EAC4 is slightly lower, the scatter patterns of stratospheric ozone tracers from both reanalysis datasets are similar to SI ozone (Fig.1), exhibiting a stronger stratospheric signal in northern sub-regions and a weaker impact on low-latitude regions.

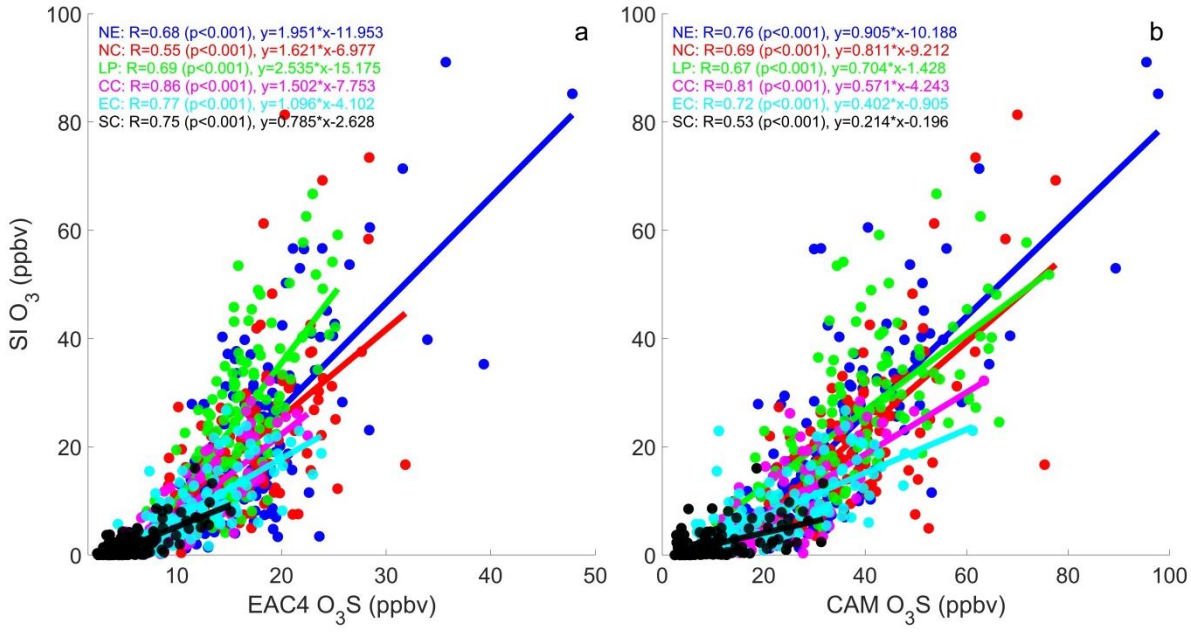

Figure 1: Scatter plots comparing FLEXPART SI ozone with a) EAC4 and b) CAM stratospheric ozone tracers (O_3S) from May to August 2019, with six different colors representing the six sub-regions.

2.4.2 Comparison with vertical structure of OMI tropospheric ozone

We examined the spatial correspondence between SI ozone and actual tropospheric ozone from the OMI remote sensing data (Figure 2). We selected OMI's measurement altitudes of 400, 600, and 850 hPa to represent the upper, middle, and lower troposphere, respectively. The vertical structure of OMI tropospheric ozone shows a distinct decrease and finer details in the troposphere with decreasing altitudes, with SI ozone exhibiting similar patterns. Horizontally, OMI ozone in the upper troposphere shows a typical north-high, south-low distribution, consistent with SI ozone (Figure 2a). In the middle troposphere, the distribution generally maintains a north-south pattern, with high ozone values extending eastward from East Asia to the western Pacific, and SI ozone responds similarly (Figure 2b). In the lower troposphere, OMI ozone shows an east-high, west-low distribution, with SI ozone displaying comparable characteristics, such as high values between 30 ℃N and 40 ℃N extending eastward from mainland China, forming a high ozone transport belt similar to the middle troposphere (Figure 2c). The vertical variations of OMI and SI ozone exhibit similar spatial patterns over CEC in the troposphere, while the simulated SI ozone concentrations are lower than OMI ozone, highlighting reasonable relationships between stratospheric impact and total ozone (SI + tropospheric production) in the troposphere and underscoring the credibility of our simulation methodology.

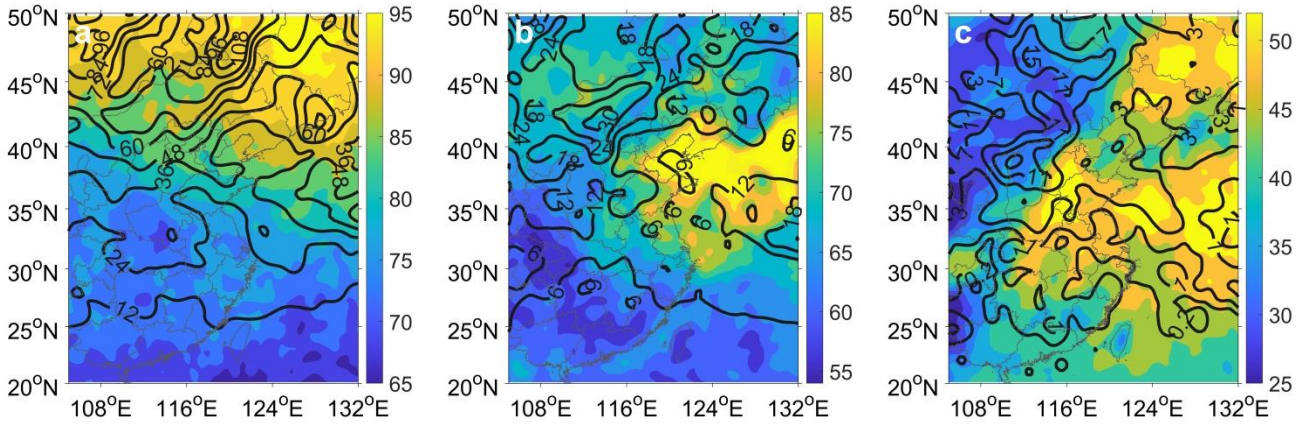

Figure 2: Spatial correspondence between SI ozone (ppbv, black contours) and actual tropospheric ozone from the OMI remote sensing data (ppbv, color contours) from May to August 2019 at altitudes of a) 400, b) 600, and c) 850 hPa.

- Detailed information on the two reanalysis datasets and Aura OMI data is provided in Section 2.1(Lines 116-149)：

2.1 Data

In this study, we utilized the meteorological fields, including geopotential height, potential vorticity, ozone mixing ratio, and wind, from the 0.75° ERA-Interim reanalysis data available from the European Center for Medium-Range Weather Forecasts (ECMWF) (https://cds.climate.copernicus.eu/cdsapp#!/dataset/reanalysis-era-interim?tab=form). ERA-Interim data are solely used for large-scale atmospheric circulation analysis, as detailed in Section 3.5. Stratospheric intrusions are primarily controlled by large-scale circulation, and our analysis using ERA-Interim data at 0.75° resolution effectively addresses the scientific issue. The daily surface ozone concentrations were obtained from the operational observations of the Ministry of Ecology and Environment of China (https://air.cnemc.cn:18007/).

The EAC4-CAMS (https://ads.atmosphere.copernicus.eu/cdsapp#!/dataset/cams-global-reanalysis-eac4) and the global atmospheric chemistry model CAM-Chem (https://www.acom.ucar.edu/cam-chem/cam-chem.shtml) both provide stratospheric ozone tracer products (O_3S) suitable for analyzing stratosphere-troposphere transport events (Akritidis et al., 2022). EAC4, the fourth-generation global meteorological and atmospheric composition reanalysis dataset released by ECMWF's Copernicus Atmosphere Monitoring Service (CAMS), includes three-dimensional fields of meteorological elements, chemical species, and aerosols (Inness et al., 2019), with a horizontal resolution of $0.75° \times 0.75°$ and 60 vertical layers. CAM-Chem, derived from the coupling of MOZART-3 stratospheric chemistry and the MOZART-4 mechanism to the Community Atmosphere Model (Tilmes et al., 2016), features a horizontal resolution of $0.9° \times 1.25°$ and 56 vertical layers.

The Aura Ozone Monitoring Instrument (OMI) Level-2 Ozone Profile data product OMO3PR is available from NASA's Goddard Earth Sciences Data and Information Services Center (GES DISC) (https://disc.gsfc.nasa.gov/datasets/OMO3PR_003/summary). The OMO3PR Level-2 ozone profile product, at a pixel resolution of 13x48 km (at nadir), is based on an optimal estimation algorithm with climatological ozone profiles as a priori information. The ozone profile is represented in terms of layer-column ozone in Dobson Units (DU) for an 18-layer atmosphere, with layers nominally bounded by pressure levels: surface pressure, 700, 500, 300, 200, 150, 100, 70, 50, 30, 20, 10, 7, 5, 3, 2, 1, 0.5, and 0.3 hPa. In this study, DU units are converted to parts per billion by volume (ppbv) using the formula: (1.2672 Ni)/Dpi 1000, where Ni represents the layer-column ozone in DU and DPi is the pressure difference between the top and bottom of each layer in hPa.

The three-dimensional ozone climate data were obtained from the Trajectory-mapped Ozonesonde dataset for the Stratosphere and Troposphere (TOST). This dataset assimilated more than 160 ozone soundings from the World Ozone and Ultraviolet Radiation Data Centre (WOUDC) using the Lagrangian method (Liu et al., 2013a). Compared to satellite ozone observations, the TOST ozone data can effectively capture the temporal and spatial variations of global stratospheric and tropospheric ozone levels, as well as the changes in ozone gradients near the tropopause (Liu et al., 2013b). The TOST dataset has a horizontal resolution of $5° \times 5°$ and a vertical resolution of 1 km, covering a range of ground to 26 km in altitude. We employed this data primarily for background climatic concentrations in the lower stratosphere when calculating the CSAII index.

- The comparison of SI events identified by simulations with ground-based observations is discussed in Section 3.3 (Lines 328-362):

3.3 Contributions of DSI and ISI to near-surface ozone

We identified DSI and ISI events occurring from May to August in 2019 based on the thresholds of near-surface SI ozone originating from the stratosphere derived from 2-day and 10-day FLEXPART trajectories, reaching 1.5 ppbv and 10 ppbv, respectively. These thresholds were determined using the 75th percentile of SI ozone concentrations. Days that did not meet these criteria were considered intrusion-free periods.

3.3.1 Comparisons between model simulations and near-surface measurements

Table 1 Agreement (in number of events) between model simulations and measured SI events in six sub-regions, along with the corresponding hit rates of simulations.

Sub-regions	Measurements	Simulations	Hit rates (%)
NE	7	5	71
NC	7	6	86
LP	32	17	53
CC	15	12	80
EC	9	8	89
SC	3	1	33

Detailed validations of simulations against surface observations are essentially important. We validated our SI assessment method using ground-based records. Chen et al. (2024) determined that significant deviations in ozone and CO from their normal values indicate an SI event if ozone concentrations at the start hour of SI exceed the seasonal mean at noon, while CO concentrations decline below their seasonal mean during the SI. Cui et al. (2009) identified SI events by observing surface ozone exceeding 10% of the 10-day running mean for at least six consecutive hours, with relative humidity below 50%. Considering the variability of moisture conditions of air parcels from higher altitudes to the surface, relative humidity is less conservative than CO (Dreessen, 2019). Thus, both high ozone and low CO values can signal a stratospheric influence (Bonasoni et al., 2000). Based on these methods, we propose a ground-based SI event identification criterion to validate the reliability of model simulations in each sub-region. The criterion involves observing near-surface ozone exceeding 10% of the 10-day running mean for at least six consecutive hours while CO concentrations are lower than the 10-day running mean. Additionally, our method considers the regional coverage for an SI event affecting near-surface air quality, which requires at least two-thirds of the total stations in a sub-region (113 to 302 stations) to meet the assessment criteria. Since the observational method cannot differentiate between types of SI, if either ISI or DSI events identified by the simulation match a measured SI event, the model is considered to have accurately hit the measured SI event.

The number of measured SI events, the number of times these events were hit by model simulations, and the hit rates are listed in Table 1. It is worth noting that the actual number of SI events simulated in this study is greater than the number of measured events hit by the model, due to the application of the stringent 6-hour ozone increase and CO decrease criterion from the literature, which results in fewer SI events. Except for the LP and CC sub-regions, the

number of measured SI events affecting near-surface ozone in other sub-regions during spring and summer 2019 is fewer than 10, consistent with Chen et al. (2024), who reported 8-12 SI events annually in China. The LP sub-region, situated on a plateau, experienced 32 SI events, comparable to the over 100 SI events reported by Cui et al. (2009) at a higher altitude site (3585 m above sea level) in Sweden. The frequency of SI events from our method aligns with these studies. Our simulation results indicate a high hit rate for SI events across all sub-regions, except for SC. The low hit rate in SC is not attributable to small PV values but rather to minimal SI impacts on this sub-region during the spring and summer of 2019, with SI not been the primary driver of elevated ozone (Oltmans et al., 2004). Therefore, the hit rate for SC is less significant.

3.3.2 Contributions of SI events to near-surface ozone

…

- Additionally, in Section 3.5, we have included an analysis of ground-based records in the context of typical Northeast Cold Vortex-induced DSI events (Lines 516-537).

Figure 11 illustrates a substantial meridional low-pressure system positioned within 2CSAl (Fig. 9), commonly recognized as the Northeast Cold Vortex (NECV). Here, we utilize this typical SI event to visually illustrate the transport process of ozone from the stratosphere into the free troposphere and subsequently into the atmospheric boundary layer driven by the NECV. This vortex stands as a prominent atmospheric system influencing the CEC, characterized by its prolonged presence as a deep, cyclonic low-pressure system of considerable intensity, primarily occurring in the spring and summer seasons. Concurrently, a robust subtropical westerly jet resides on the southern flank of the NECV (30 °-40 ° N). On May 19, the SI ozone was predominantly situated north of 35 ° N, with the majority of stratospheric air particles concentrated within the middle troposphere (Figure 11a). By May 20, the stratospheric air particles exhibit southeastward movement, following the trajectory of the NECV (Figure 11b). Subsequently, a substantial portion of stratospheric ozone has permeated the lower troposphere, with some particles detected at altitudes below 500 m. On the 20th, an observed increase in near-surface ozone and a reduction in CO persisted for an average of 8 hours across vast areas in central CEC, which is also reflected in the distribution of stratospheric air in the boundary layer and the spatial correspondence of the SI vertical structure (Figures 10b and 10d). The vertical depiction of atmospheric circulation and ozone concentrations in Figures 11c and 11d underscores the deep tropopause folding near the NECV, extending downward to 500 hPa. A robust downdraft is evident below the folding zone, facilitating the descent of high-level stratospheric ozone towards the boundary layer (Fig. 11d). This aligns with the simulated trajectory in this study (indicated by the symbol '+' in Figure 11b). The impact of this DSI event primarily affected the LP, NC, CC, and EC regions, resulting in SI ozone concentrations of 11.4, 6.1, 6.1, and 11 ppbv, respectively. NE also experienced the effects of the DSI event, observing SI ozone concentrations of 4.7 ppbv. However, the influence on SC remained negligible, with SI ozone levels below 0.4 ppbv. A prior study by Chen

et al. (2014) highlighted the propensity of the NECV to induce stratosphere-troposphere exchange over the NE region. Our study contributes to a new understanding by revealing that the NECV can provide an exceptional pathway for ozone transport across the tropopause and a deep intrusion, leading to significant DSI impacts of daily scales in CEC.